Ceramics International 47 (2021) 20019–20031

Contents lists available at ScienceDirect

Ceramics International

journal homepage: www.elsevier.com/locate/ceramint

Toward a better understanding of multifunctional cement-based materials: The impact of graphite nanoplatelets (GNPs)

Francesca R. Lamastra [a,*], Mehdi Chougan [a,b], Emanuele Marotta [a], Samuele Ciattini [c], Seyed Hamidreza Ghaffar [b], Stefano Caporali [d], Francesco Vivio [a], Giampiero Montesperelli [a], Ugo Ianniruberto [e], Mazen J. Al-Kheetan [f], Alessandra Bianco [a]

[a] Università di Roma "Tor Vergata", Dipartimento Ingegneria dell'Impresa "Mario Lucertini", Consortium INSTM RU "Roma Tor Vergata", Via del Politecnico, 00133, Roma, Italy
[b] Department of Civil and Environmental Engineering, Brunel University London, Uxbridge, UB8 3PH, United Kingdom
[c] Università di Firenze, Centro di Cristallografia Strutturale "CRIST", Via della Lastruccia 3, 50019, Sesto F.no, Italy
[d] Università di Firenze, Dipartimento di Ingegneria Industriale "DIEF", Consortium INSTM RU "Firenze", Via di Santa Marta 3, 50139, Firenze, Italy
[e] Università di Roma "Tor Vergata", Dipartimento di Ingegneria Civile ed Informatica (DICII), Viale del Politecnico, 00133, Roma, Italy
[f] Civil and Environmental Engineering Department, Mutah University, Mutah, Karak, 61710, P.O. BOX 7, Jordan

ARTICLE INFO

Keywords:
Cementitious nanocomposites
Graphite nanoplatelets (GNPs)
Mechanical properties
Microstructure
Resistivity
Thermal conductivity

ABSTRACT

The impact of graphite nanoplatelets (GNPs) on the physical and mechanical properties of cementitious nanocomposites was investigated. A market-available premixed mortar was modified with 0.01% by weight of cement of commercial GNPs characterized by two distinctively different aspect ratios.

The rheological behavior of the GNP-modified fresh admixtures was thoroughly evaluated. Hardened cementitious nanocomposites were investigated in terms of density, microstructure (Scanning Electron Microscopy, SEM and micro–Computed Tomography, μ-CT), mechanical properties (three-point bending and compression tests), and physical properties (electrochemical impedance spectroscopy, EIS and thermal conductivity measurements). At 28 days, all GNP-modified mortars showed about 12% increased density. Mortars reinforced with high aspect ratio GNPs exhibited the highest compressive and flexural strength: about 14% and 4% improvements compared to control sample, respectively. Conversely, low aspect ratio GNPs led to cementitious nanocomposites characterized by 36% decreased electrical resistivity combined with 60% increased thermal conductivity with respect to the control sample.

1. Introduction

Cement-based materials (CBMs) are ubiquitous in the realization of infrastructures, roads, buildings, oil and gas wells, and offshore implants. The global cement market is expected to reach USD 682.3 billion by 2025 [1].

However, despite such prolonged and extensive use, conventional CBMs typically exhibit poor tensile strength due to the presence of flaws and microcracks mainly associated with excess water, bleeding, plastic settlement, and shrinkage [2,3]. Under applied loads, these pre-existent defects propagate and coalesce, resulting in macrocracks that lead to mechanical instability and, finally, catastrophic failure. The formation of cracks is also responsible for an increased tendency to degradation damage caused by freeze-thaw cycles and increased exposure to aggressive environmental agents [4,5].

Many types of research have focused on the incorporation of graphene-based materials (GBMs) in the cement matrix to enhance the strength and durability of the resulting nanocomposites [6–10].

The GBMs' crucial role in accelerating cement hydration, pore refining and reducing flaws and cracks in a CBM has been clearly assessed in the literature [11–14]. Moreover, the addition of thermally conductive fillers, including GBMs, reduces the risk of early-age cracking [15] and also enables the development of cement-based "smart materials", defined as materials that respond to an external physical or chemical stimulus in a controlled manner to conduct a predetermined task [16,17].

Conductive cement-based nanocomposites belong to this class of material, since the presence of the electrically conductive fillers enables

* Corresponding author.
E-mail address: lamastra@scienze.uniroma2.it (F.R. Lamastra).

https://doi.org/10.1016/j.ceramint.2021.04.012
Received 8 February 2021; Received in revised form 30 March 2021; Accepted 1 April 2021
Available online 3 April 2021

a piezoresistive self-sensing ability [18,19].

As the nanocomposite experiences a certain deformation in response to a stress, the "state" of the interphase between the filler and the matrix changes, affecting the electrical resistance of the overall cementitious materials. Hence, cracks and damages can be detected by measuring the electrical resistance. The piezoresistive responses of conductive cement composites depend on several factors, such as the raw materials, mix proportions, the type, shape, and degree of dispersion, and content of the electrically conductive filler [20–22]. In this work, multifunctional cement mortar nanocomposites were produced by adding graphite nanoplatelets (GNPs) as the electrically and thermally conductive fillers. GNPs consist of multiple stacked graphene layers bonded by van der Waals forces, resulting usually in micrometer-wide slabs up to 150 nm thick. Among GBMs, GNPs are particularly interesting since they combine mechanical properties (in-plane elastic modulus 1 TPa, strength 130 GPa), electrical conductivity ($5.98 \cdot 10^4$ S/m), and thermal conductivity (3000 W m^{-1} K^{-1} in-plane, 6 W m^{-1} K^{-1} along z-axis) comparable to 2D graphene (in-plane elastic modulus 1 TPa, strength 130 GPa, electrical conductivity $7.2 \cdot 10^3$ S/m, and in-plane thermal conductivity 5300 W m^{-1} K^{-1}) [23–25] with a low cost, especially for large-scale applications [26,27].

However, the dispersibility of GNPs is usually rather poor in water media, as their hydrophobic nature leads to a strong tendency to form large agglomerates [6,25]. In this respect, previous studies reported that low dosages (i.e. 0.01–0.05% by weight of cement) of GBMs were more effective in improving the mechanical strength and/or physical properties of the resulting cement-based nanocomposites than high dosages (i.e. 0.1–0.4% by weight of cement) [13,26,28]. This is simply due to a reduced agglomeration and enhanced distribution of the nanofiller.

In this paper, the impact of a minimum amount (0.01% by weight of cement) of two commercial GNPs, distinctly different in terms of aspect ratio, on the rheology, microstructure, and properties (strength, electrical resistivity, and thermal conductivity) of the resulting nanocomposites is thoroughly investigated.

To the best of the authors' knowledge, a study focused on the correlation of GNP microstructure with the mechanical and physical properties of the subsequent cementitious nanocomposites has not yet been conducted.

2. Materials and methods

2.1. Materials: EN 998-2 mortars and GNPs

A commercially available EN 998–2 premixed dry mortar (class M5) consisting mainly of Portland cement, graded sand, and hydrated lime was used in this study. Particle size was below 3 mm and the composition followed ASTM C109; that is, one part Portland cement type (I), two parts sand, and 0.75 parts lime (by weight) [26,28].

The compositional and microstructural features of *G2Nan* and *G4Nan* (*Nanesa, Italy)* used herein as the nanofiller source are reported in Table 1. The microstructure of the GNPs was investigated using Scanning Electron Microscopy (SEM*; LEO Supra 35, Germany*). For such a purpose, as-received GNP water paste (about 50 mg for *G2Nan* and 15 mg for *G4Nan*) was added to 250 mL of acetone. The mixture was then ultra-sonicated for 30 min (*Sonics Vibra-Cell* tip sonicator, mod. VC 750, USA), drop-casted onto the microscope stub, and, finally, air-dried at room temperature. Further characterization details have been reported in a previous study by authors [26].

2.2. Fresh GNP-modified admixtures: preparation and rheology measurements

A suitable amount of water (18% wt) was added to the EN-998-2 premixed mortar following the producer's instructions. The as-received *G2Nan* or *G4Nan* water paste was then directly added to the fresh mixture. Based on a previous study by authors [26], the EN-998-2 premixed mortar has been modified with 0.01% GNPs by weight of cement. The resulting admixtures were named G2 and G4, respectively.

Lastly, in accordance with ASTM C305-06, the admixtures were mechanically stirred for 5 min at 500 rpm utilizing *Eurostar digital (IKA®-Werke, Germany)* equipped with a spiral stirrer *IKA®-Werke (Germany)*. Rheology measurements of neat and modified fresh mortars were performed immediately after the mechanical mixing utilizing the *Kinexus Lab* + rheometer (*Malvern Instruments Ltd., UK*) equipped with the software *rSpace (Malvern Panalytical Ltd, UK)*. Fresh mortars were poured into a cylindrical plastic jar (diameter 12 cm); shear stress and apparent viscosity were recorded in the shear rate range of 0.1 s^{-1}-100 s^{-1} over 22 intervals.

2.3. GNP-modified nanocomposites: casting and hardening

In accordance with ASTM C348-02 standard, neat and GNP-modified mortar samples of size 40 mm × 40 mm x 160 mm were cast in a steel mold previously coated with hydraulic oil, mechanically vibrated (*Retsch, Germany*) for 3 min, and finally stored in air under a wet cloth for 24 h. Samples were then removed from the mold and kept in water at room temperature for 7, 14, and 28 days. The resulting cementitious nanocomposites loaded with *G2Nan* or *G4Nan* were herein designated as G2 and G4, respectively.

2.4. GNP-modified nanocomposites: density, mechanical properties, and microstructure

The density of the hardened mortars was determined by weight (*Mettler-Toledo Ltd.*) and size measurements (digital calliper). Mechanical tests were performed according to the ASTM C348-02 and ASTM C349-02 standards, respectively: three-point bending was done using an MTS (USA) machine equipped with a 100 kN load cell, and compression employing a *Matest* machine (*Italy*); latter tests were performed at 0.1 mm/min rate using a 3000 kN load cell. Flexural strength was evaluated from the load *versus* crosshead displacement curve resulting from the three-point bending tests, following ASTM D790.

In conformance with ASTM C348-02 and ASTM C349-02, three and six specimens were considered for each sample, for the bending test and compression test, respectively.

The microstructure of the samples hardened for 28 days was thoroughly investigated using SEM. A total of ten specimens (size around 5 mm × 5 mm x 5 mm) for each type of sample were collected from central

Table 1
Purity, size, thickness, specific surface area (SSA), aspect ratio, and GNP content in the water paste (wt.%) of G2Nan and G4Nan graphite nanoplatelets (courtesy of Nanesa).

Designation	Carbon (wt%)	Average lateral size and/or size distributions	Thickness	Layers	Aspect ratio	SSA (m^2/g)	GNP content in the water paste (wt.%)
G2Nan	97 (C:O = 44:1)	30 μm D_{50}:25 μm	14 nm	40	1786	>30[a]	5.9[b]
G4Nan	>97 (C:O = 49:1)	D_{50}:42 μm D_{90}:96 μm	8 nm	17	5250	56[a]	20[b]

[a] Measured through N_2 adsorption (BET method) on dry powders.
[b] Evaluated by thermogravimetry.

parts of fractured specimens after compression tests, dried in an oven at 110 °C for 3 days, stored in ethanol, and finally gold-coated by sputtering *(EMITECH K550X sputter coater, Quorum Technologies Ltd, UK)*.

Micro-computed tomography (μ-CT) analysis was performed on made-on-purpose cubic samples of size 20 mm hardened for 7, 14, and 28 days. The samples were analyzed by collecting μ-CT data using *Skyscan 1172* high-resolution microCT. This system has a sealed, microfocus tungsten X-ray tube with a 5 μm focal spot size. The X-ray was produced by exposing the anode to an electron beam at a range of 100 kV and 100 μA with Al + Cu as primary filters. Each sample was placed on a pedestal between the X-ray tube source and the charge-coupled device detector. The 2D X-ray images were captured with a slice-to-slice rotation angle range of 0.5°. The total acquisition time was approximately 40 min. The spatial resolution of the images was kept at 32 μm in terms of pixel size. The 3D image of the object's internal structure was reconstructed using a modified *Feldkamp algorithm* for cone-beam acquisition geometry, realized in *Nrecon* v.1.6.3.3 software. The alignment and beam hardening corrections were made before starting the re-construction process. *CTVox* and *CTVol* programs were used for 3D visualization, while CT-Analyser (*CTan*) software was used for the image clean up and measurements.

2.5. GNP-modified nanocomposites: electrochemical impedance spectroscopy (EIS)

The aim of the EIS tests was to evaluate the effect of GNPs on the electrical resistivity of the cement-based nanocomposites in the steady-state condition. EIS tests were performed on 40 mm × 40 mm x 160 mm bars hardened for 7, 14, and 28 days.

EIS tests (*VMP3, BioLogic Science Instruments, France*) were carried out by applying an alternate signal (amplitude 20 mV and frequency range 10 mHz–100 kHz), using a uniaxial two-point electrode method (Fig. 1). A wet sponge was placed between the sample's outer surface and the copper electrodes to ensure complete contact.

The resistivity (ρ) of the cement-based nanocomposites was calculated from Z', the highest real resistance value, employing equation (1) [21,29,30]:

$$\rho = \frac{R \cdot S}{L} \tag{1}$$

where: R is the sample resistance, S is the sample's cross-section, and L is the distance between the two electrodes.

It is well known that a small change in the saturation level will affect the conductivity (or resistivity) of the mortars as it leads to variation in the amount of water trapped in the porous network. In order to obtain reliable and repeatable measurements, EIS was then performed on samples in a saturated surface dry (SSD) condition [29].

Statistical evaluation was carried out by the means of Minitab® 14 statistical software to validate the accuracy of the output data with standard deviation.

2.6. GNP-modified nanocomposites: thermal conductivity

Thermal conductivity measurements were performed using a heat flow meter *(LaserComp Fox 200, Laser Comp, Inc.)* equipped with *Win-Therm32* software for data collection and analysis, in accordance with ASTM C 518 and EN 12667. For each sample hardened for 28 days, three different specimens (100 mm × 100 mm × 20 mm) were tested with the temperature settings at 0 °C and 20 °C, for the top cold plate and the bottom hot plate, respectively.

3. Results and discussion

3.1. G2Nan and G4Nan: size, morphology, and topography

As expected, SEM micrographs of both *G2Nan* and *G4Nan* showed micro-sized agglomerates of nanoplatelets (Fig. 2); folded and crumpled morphologies were detected, particularly for *G4Nan*.

A significant reduction of the lateral size was observed with respect to the information furnished by the producers (Table 1). In accordance with the literature, such effect was induced by the tip sonication process [31].

3.2. GNP-modified fresh admixtures: rheological behavior

Since it is well known that the workability of fresh cementitious admixtures modified with GBMs might be compromised [15,32], the rheological characterisation was performed.

The flow curves obtained for G2 and G4 cementitious fresh admixtures are presented in Fig. 3.

A modified Bingham model was adopted to fit the shear stress-shear rate data of curves (equation (2)) [33]:

$$\tau = \tau_0 + \eta_p \cdot \gamma + c \cdot \gamma^2 \tag{2}$$

where: τ, τ_0, η_p, γ and c are the shear stress, yield shear stress, plastic viscosity, shear rate, and a regression constant, respectively. This model

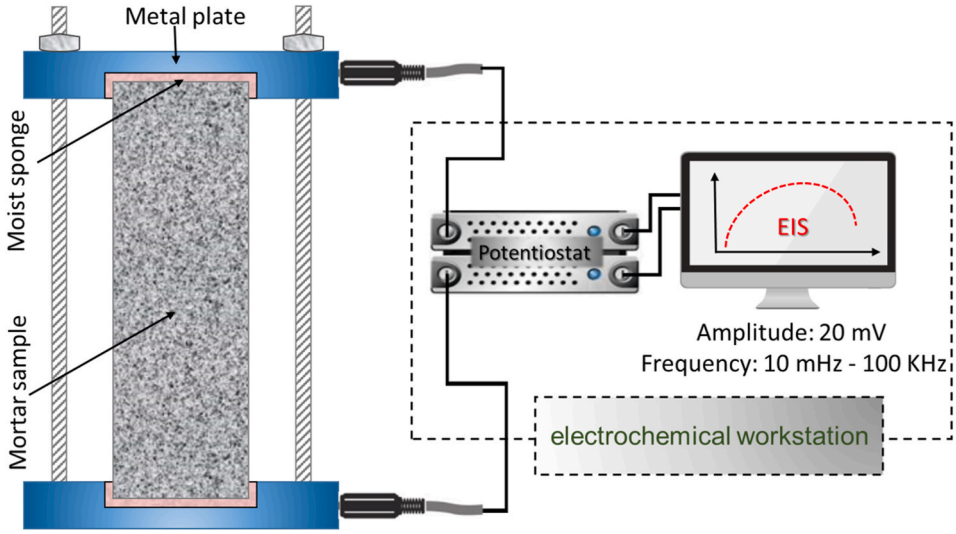

Fig. 1. Uniaxial two-point electrode method.

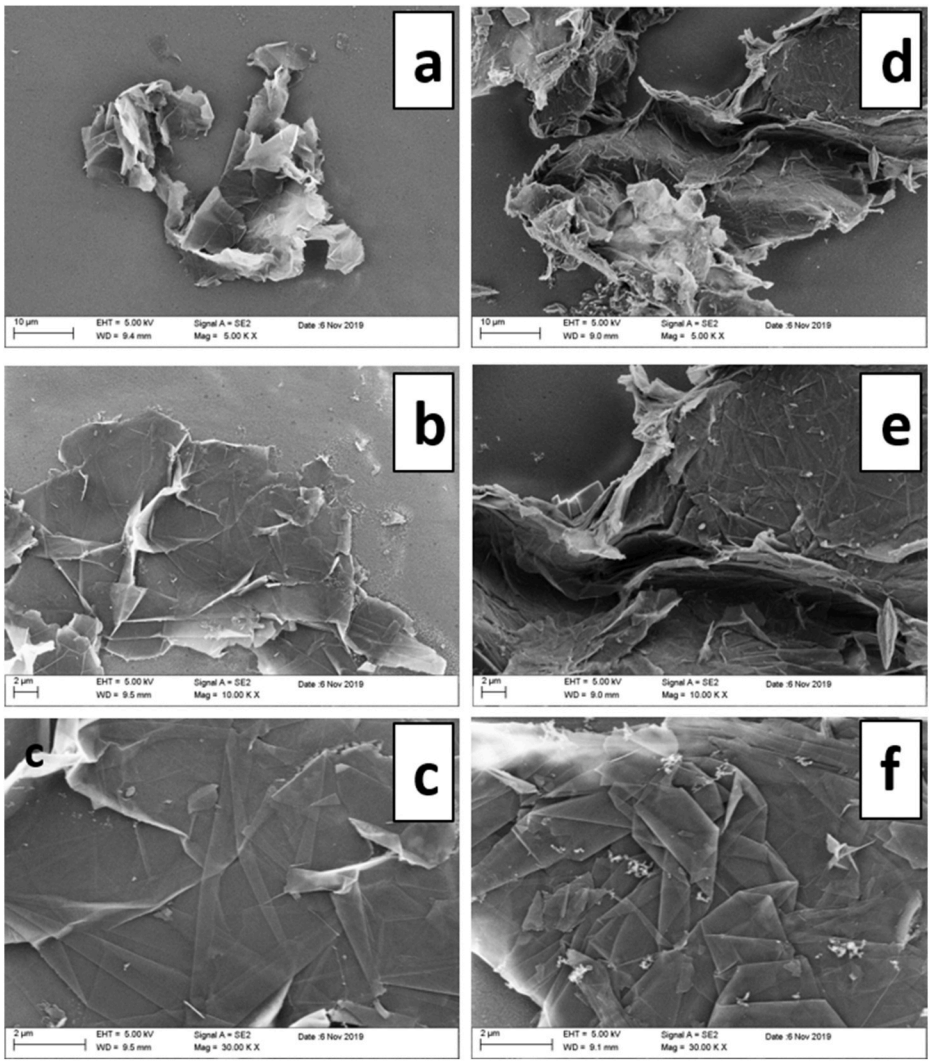

Fig. 2. Scanning electron microscopy (SEM) micrographs at a different magnification of *G2Nan* (low aspect ratio GNPs) (a,b,c) and *G4Nan* (high aspect ratio GNPs) (d,e,f).

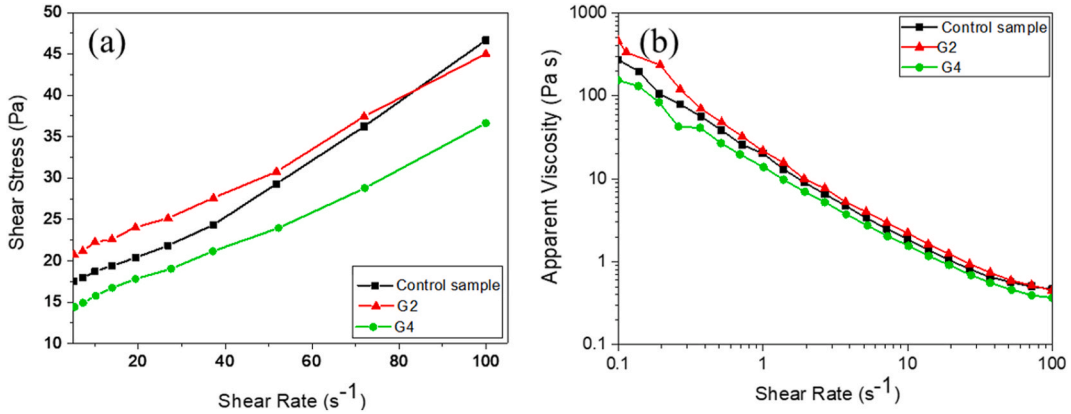

Fig. 3. Rheological behavior ((a) shear stress *vs* shear rate and (b) apparent viscosity *vs* shear rate) of neat and GNP-modified fresh admixtures.

has been widely used to describe the flow curves of neat and GNP-modified cementitious mixtures needing a shear stress higher than a threshold value (i.e. τ_0) to start flowing and behave as pseudoplastic fluids [26,28,34,35].

The resulting rheological parameters (*i.e.* yield shear stress, τ_0; plastic viscosity, η_p), and correlation coefficients (R^2) are reported in Table 2.

For the G2 admixture, a higher shear stress to start flowing (τ_0) and a slightly higher plastic viscosity (η_p) (*i.e.* flow resistance) were observed (Table 2). A reduced workability should then be expected with respect to

Table 2
Rheological properties of the neat and GNP-modified fresh admixtures.

Sample	Fitting Equation ($\tau = \tau_0 + \eta_p \cdot \gamma + c \cdot \gamma^2$)	τ_0 (Pa)	η_p (Pa·s)	Correlation coefficent (R^2)
Control sample	$y = 0.0012x^2 + 0.1745x + 16.60$	16.60	0.1745	0.9987
G2	$y = 0.0007x^2 + 0.1841x + 19.89$	19.89	0.1841	0.9978
G4	$y = 0.0006x^2 + 0.1684x + 13.94$	13.94	0.1684	0.9976

the control sample. Reasonably, such an effect has to be associated with the wetting of the *G2Nan* platelets (Table 1), which led to a reduction of free water in the cementitious admixture, thereby increasing the friction among the particles.

Conversely, according to the data reported in Table 2, *G4Nan* induced a decrease of the flowability parameters, thus suggesting improved workability of the fresh cementitious admixture with respect to the control sample. In this case, most probably because of the larger lateral size of *G4Nan* (Table 1), the lubricating effect overcomes the thickening action. A beneficial effect on the flowability of cement-based fresh admixtures associated with the presence of GNPs has been reported in the literature at higher nanofiller content (i.e. >0.05 wt%; see, for example [26,32]). This behavior is due to the ease with which stacked graphene layers in GNPs slide over each other, resulting in the self-lubrication properties of the 2D nanofiller. In this study, the impact of self-lubricating platelets on flowability was observed at very low GNP content (0.01 wt%); the observed phenomenoun could be mainly related to mortar granulometry and platelet lateral size.

3.3. GNP-modified nanocomposites: density and mechanical properties

Results of density measurements and mechanical tests performed on G2 and G4 nanocomposite mortars hardened for 7, 14, and 28 days are illustrated in Fig. 4a–c.

All samples showed improved density, already reached at 7 days; values were comparable to those observed at 200 days for the control sample, whose peculiar densification behavior has already been discussed elsewhere [28]. The various evolutions of density, clearly evidenced in Fig. 4a, could be linked to the different degrees of mass *versus* volume reduction over the hydration time [36].

At 28 days, according to our previous studies and several other authors [15,26,28,37], both G2 and G4 nanocomposite mortars showed about 12% increased density compared to the control sample. Such a result could be due to the heterogeneous nucleation of calcium silicate hydrate (C–S–H) onto the GNPs combined with the simultaneous pore refinement effect, also associated with the presence of nanofiller [37,38] (This latter issue will be extensively discussed in paragraph 3.4.). Moreover, the observed density trend clearly suggests that *G4Nan,* characterized by a higher aspect ratio (Table 1), is more effective than *G2Nan* and thus clearly results in an accelerated hydration process (Fig. 4a).

Regarding the mechanical properties, all samples, except for G4 at 14 days, showed improved compressive (R_c) and flexural (R_b) strength (Fig. 4b and c).

At 28 days, both G2 and G4 nanocomposite mortars showed a moderate improvement in compressive strength (*i.e.* of 6% and 14%) with respect to the control sample. In the same condition, the flexural strength was nearly unaffected (*i.e.* less than 5%) by the incorporation of GNPs.

At 7 days, conversely, the strengthening effect due to the presence of the GNPs was clearly evidenced for both G2 and G4 nanocomposites: the

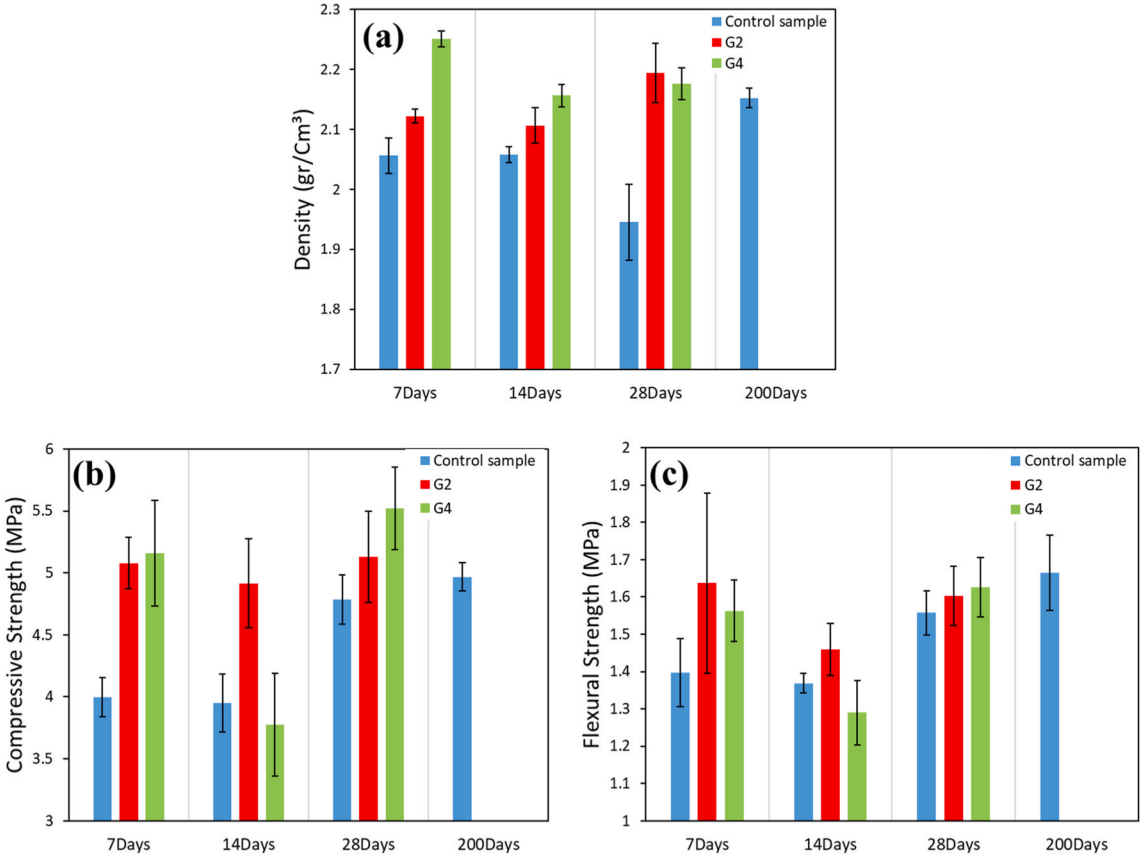

Fig. 4. Density (a), compressive strength (b), and flexural strength (c) of GNP-modified mortars.

R_c values had increased by 28% and 30% and the R_b ones by 17% and 11%, compared to the control sample.

These results suggest that an adequate nanofiller dispersion had been achieved along with the development of a strong nanofiller/matrix interface; the latter effect is further enhanced by the incorporation of higher aspect ratio platelets (*i.e. G4Nan*) [6,7].

Several other effects might be responsible for the strengthening observed in GNP-modified cementitious nanocomposites including pore refinement, and the "bridging effect" [6,39].

Lastly, a reduction of the mechanical properties at 14 days was observed for nanocomposite mortars, remarkable for the case of G4 sample (Fig. 4b). This behavior could be due to the greater effect of higher aspect ratio GNPs (*G4Nan*) on the C–S–H growth kinetics, the resulting microstructure-determined by the non-regular spatial crystalline framework, associated with the shape and size of hydration products [13,40]- and the development of the consequential capillary pore network.

3.4. GNP-modified nanocomposites: microstructure

SEM micrographs of the two GNP-modified mortars are presented in Fig. 5. The honeycomb structure of C–S–H, the polygonal crystals of portlandite, and the needle-like crystals of ettringite were observed in all samples. At a specific microscale level, the incorporation of GNPs seems not to significantly affect the microstructure of the cementitious matrix nanocomposites.

A high-magnification SEM micrograph (Fig. 6) showed a folded *G4Nan* nanoplatelet (Fig. 2) among the cement granules. According to the literature, the observed lateral size of the nanoplatelets is, interestingly, much smaller than that declared by the supplier (Table 1). The effect reasonably stems from mechanical mixing of the fresh admixtures, where shear stresses induce reduction of the lateral dimension of the 2D filler and GNP exfoliation, creating thinner structures [41].

It is worth mentioning that the chance of identifying a GNP within the cement matrix is rather rare, particularly for the chosen minimum dosage of nanofiller (*i.e.* 0.01% by weight of cement) [28,42].

To inspect the impact of the GNPs on the microstructural evolution of the nanocomposites, μ-CT analysis was performed. μ-CT is particularly advantageous for the study of the microstructural development of cementitious materials; it is at the same time feasible, versatile, non-invasive, and non-destructive compared to other conventional techniques such as mercury intrusion porosimetry (MIP) or SEM.

Conversely, three-dimensional μ-CT analysis can also be considered complementary to SEM and/or MIP since it provides unique qualitative

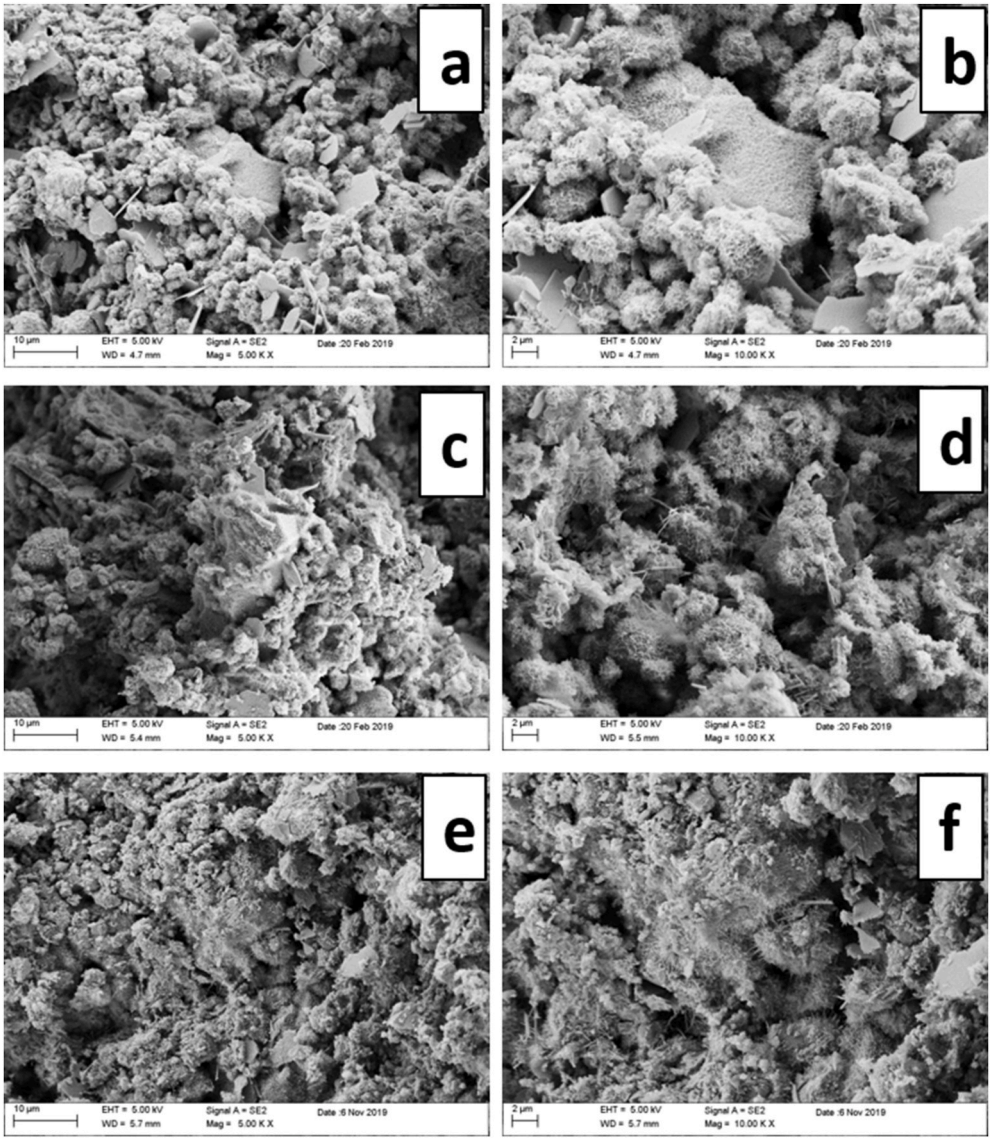

Fig. 5. SEM micrographs of mortars hardened for 28 days (a,b) control sample, (c,d) G2 sample, and (e,f) G4 sample.

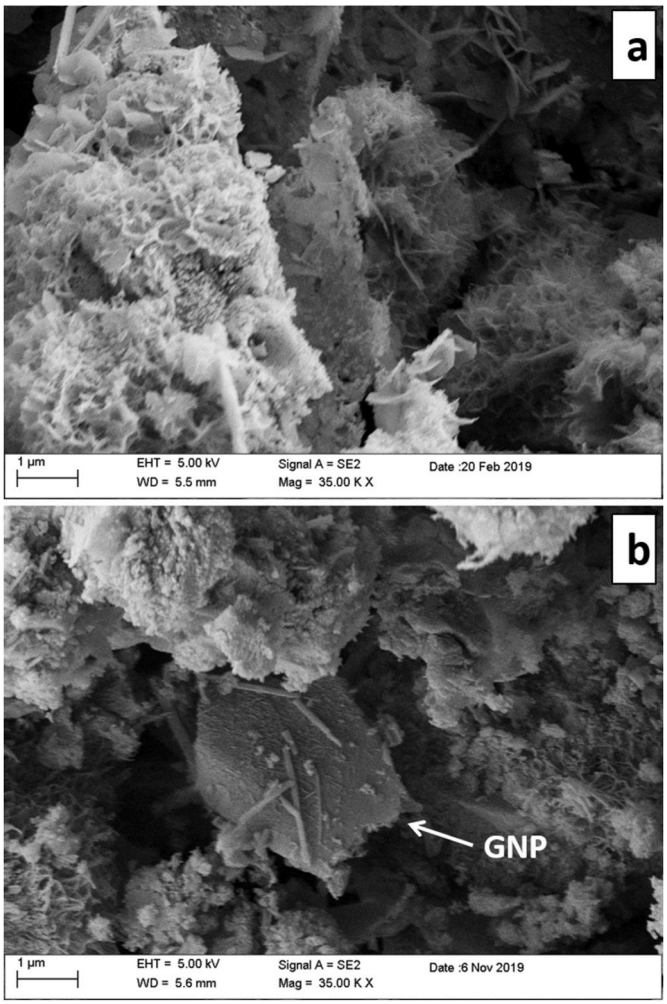

Fig. 6. High magnification SEM micrographs of GNP-modified mortars at 28 days (a) G2 and (b) G4.

and quantitative information, e.g., pore network and spatial heterogeneity [43–45].

However, depending on the adopted resolution scan, the smallest detectable pore size is about 30 µm. The porosity of CBMs can be grouped into: *(i) gel pores* (from a few nm to 0.2 µm; minor role in transport processes); *(ii) capillary pores* (from 0.2 µm to 10 µm; mainly involved in transport properties); and *(iii) air voids* (above 10 µm; a small fraction of isolated heterogeneities that play a minor role in transport processes) [44]. Hence, the capillary pore network is the main factor affecting the performance of cementitious materials in terms of interactions with the environment which, in turn, determines their durability. In this regard, the connectivity of the capillary pore network is essential in defining the service life of the material.

Thus, the porosity determined by µ-CT analysis is expected to be remarkably underestimated since the spatial resolution does not allow detection of either gel pores or most of the capillary pores, the latter representing up to 70–90% of the whole pore volume of the cement paste [43,44,46,47].

Results of µ-CT analysis performed on samples hardened at 7, 14, and 28 days are reported in Table 3, while selected 3D µ-CT images are presented in Fig. 7.

The obtained values of *total porosity* showed a progressive decrease with the hardening time. More specifically, at 28 days, the *total porosity* of the control sample and the G2 mortar showed a 47% and 62% decrease, respectively, compared to samples hardened for 7 days. *Open porosity* followed the same trend; it decreased for both the control and the G2 mortar, by 50% and 83%, respectively, compared to early aged samples (*i.e.* 7 days).

Table 3
Results of µ-CT analysis for the neat mortar (control sample) and the G2Nan-modified mortar (G2) hardened for 7, 14, and 28 days.

Description	*Control sample*			*G2*		
	7 d	14 d	28 d	7 d	14 d	28 d
Closed porosity (%)	1.3	1.3	0.7	1.1	3.2	3.2
Open porosity (%)	0.2	0.1	0.1	12.8	3.9	2.1
Total porosity (%)	1.5	1.4	0.8	13.9	7.1	5.3

However, *closed porosity* data showed an opposite trend: a remarkable increase for G2 (190%) and decrease for the control sample (46%) (Table 3).

The µ-CT investigation enabled the assessment of the effect of GNP incorporation on the microstructure of nanocomposites. It was shown that *G2Nan* led to an increased *open porosity* of mortar at 7 days by two orders of magnitude (with respect to the control sample). This is most likely due to improved reactivity of cement particles in the proximity of the GNPs, which promotes heterogeneous nucleation of the C–S–H phase. Such a microstructural feature, despite remarkable reduction due to the hydration process, is partially maintained even at 28 days (compared to the control sample). Therefore, for G2 an improved interconnectivity of the pore network is expected, even at later ages. This hypothesis was further fully supported by the distinct electrical behavior of the G2 compared to the control sample.

To the best of the authors' knowledge, the impact of GNPs on the *open porosity* of cement mortar has not been previously reported in the literature. By using µ-CT, the obtained values of *total porosity* are in agreement with those reported for neat cementitious materials (i.e. 1.8% for a voxel size of 1.81 µm [44], 5% and 6.6% for a voxel size of 2.67 µm and 2 µm, respectively [45]).

The pore size distribution obtained by µ-CT measurements is reported in Fig. 8.

Regarding the early-aged control sample, the detectable pore sizes were mainly distributed in two ranges, i.e. between 0.034 and 0.103 mm (% volume 63.05), and between 0.103 and 0.172 mm (% volume 17.41). The percentage volume occupied by small pores, i.e. in the range 0.034–0.103 mm, significantly decreased with hardening, reducing by 76%. On the other hand, at 28 days the percentage volume of pores larger than 0.103 mm increased by 130%.

Interestingly, for the early-aged G2 sample, the main contribution to the detected porosity was in the ranges 0.017–0.052 mm and 0.052–0.086 mm, representing 41.56% and 46.4% of the total pore volume, respectively. Such a result suggests that the addition of GNPs increases the fraction of the smaller detectable pores at an early age: that is, pores smaller than 0.086 mm represent 87.96% pore volume for the G2 sample, and pores smaller than 0.103 mm represent 63.05% for the control sample.

For the G2 sample, the percentage volume of smaller pores also remarkably decreased with hardening (a reduction by 100% and 98% for pores in the ranges 0.017–0.052 mm and 0.052–0.086 mm, respectively). Moreover, for the pores larger than 0.086 mm, they increased by 720% compared to the early age.

For both samples at 28 days, the pore size distribution shifted towards larger dimensions and pores were more uniformly distributed over the various diameter ranges, compared to the early age. The effect is more noticeable in the case of the G2 sample.

3.5. GNP-modified nanocomposites: electrical resistivity

In this study, the electrical characterization of neat and GNP-modified mortars was performed by EIS.

The resistivity data of neat and GNP-modified mortars hardened for

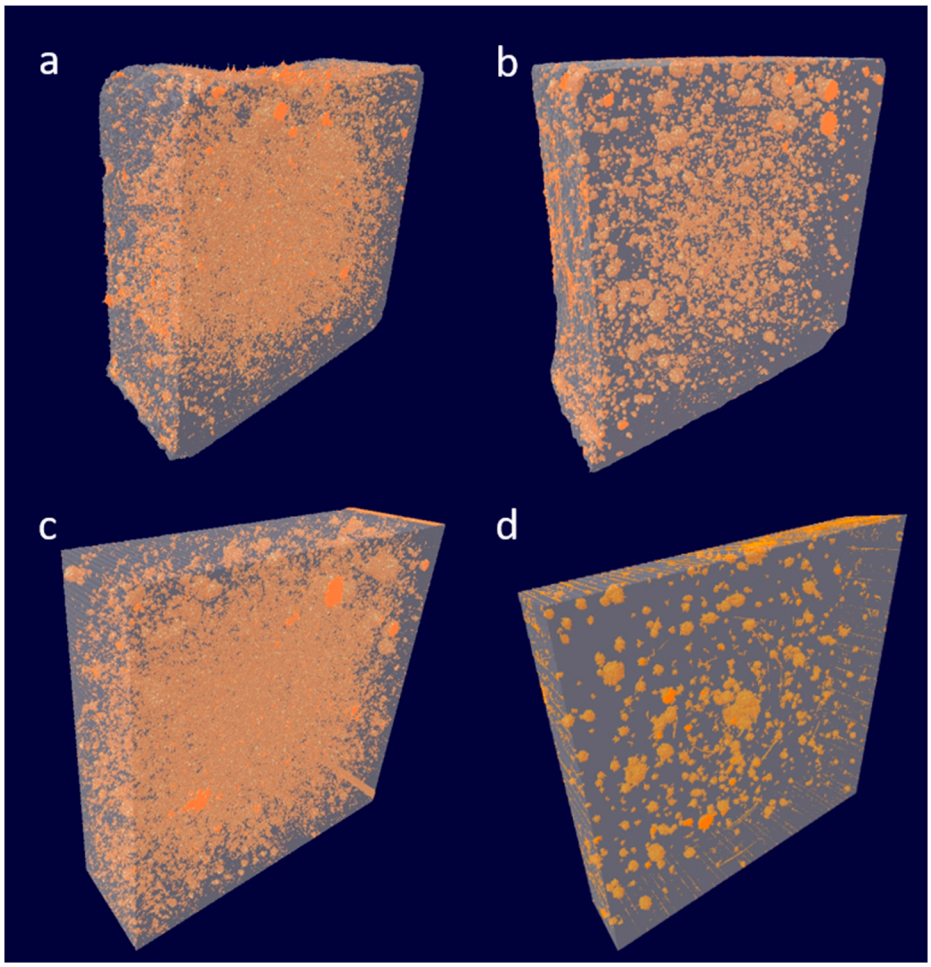

Fig. 7. 3D μ-CT images of mortars (a) control sample at 7 days, (b) control sample at 28 days, (c) G2 at 7 days and (d) G2 at 28 days.

7, 14, and 28 days are presented in Fig. 9.

The resistivity of G4 and the control sample followed the same trend, progressively increasing with the hardening time and reaching 1030 Ω m and 867 Ω m, respectively, at 28 days.

According to the literature, moist mortars behave as semiconductors with a resistivity of the order of 10^5 Ω mm [29].

The observed electrical behavior of GNP-filled cementitious composites is the result of the following conduction mechanisms: (*i*) *ionic conduction*-owing to ionic motion through the free evaporable water located in the interconnected capillary pore network of the cementitious matrix, which then progressively decreases with the hardening time; (*ii*) *tunneling conduction:* associated with the transmission of electrons among "disconnected", but close enough, conductive nanoparticles, which takes place when the electrons actually "jump" from one GNP to another, by-passing the energy barrier opposed by the interposed cementitious matrix; and (*iii*) *contacting conduction*-caused by the direct contact of neighboring nanoplatelets, thus resulting in the development of a conductive network [15,48].

Regarding electrical resistivity, the trend observed in Fig. 9 suggests that the mortar reinforced with 0.01%wt of *G4Nan* does not reach the *percolation transition zone* and, thus, ionic conduction dominates; therefore, G4 and the control sample exhibit comparable resistivity at 28 days. It is worth mentioning that the high standard deviation, obtained for G4 at 28 days, might be due to the presence of microstructural inhomogeneities coming from the incorporation of higher aspect ratio nanoplatelets [49].

The addition of *G2Nan* to the premixed mortar induced the opposite trend: the electrical resistivity progressively decreased with hydration time and reached 556.7 Ω m at 28 days, a remarkably lower value compared to the control sample, *i.e.,* reduction of 36%.

It is reasonable to ascribe such an effect to a more homogeneous dispersion of the lower aspect ratio *G2Nan,* which somehow led to a favorable distribution and/or orientation of the conductive nanofiller in the cementitious matrix [15,37,50]. Because higher levels of GNP exfoliation, induced by shear stresses during mixing, are expected for the lower aspect ratio filler, better dispersion of *G2Nan* in the cementitious matrix had presumably been achieved, which resulted in conductive pathways.

Moreover, in aiming to fully understand the distinctly dissimilar electrical response of the two nanocomposite mortars loaded with GNPs of different aspect ratios, the EIS spectra were analyzed using *equivalent circuit models* proposed as in the literature for cementitious systems [51], with the fitting efficiency being evaluated by means of *Chi-squared* values. The results are reported in Table 4; the Nyquist plots and the equivalent circuits are presented in Fig. 10.

According to Fig. 10, the Nyquist plots show non-ideal semi-circles, the effect being most probably due to microstructural inhomogeneity typical of cementitious materials as previously shown in Figs. 5 and 6 [52].

To take into account the expected deviation from the ideal behavior, the chosen equivalent circuits include both purely resistive elements (R) and constant phase elements (CPE), the latter modelling the behavior of a double-layer that is considered an imperfect capacitor. In more detail, the CPE is a complex circuit component with a frequency-dependent impedance that can be expressed by the following equation:

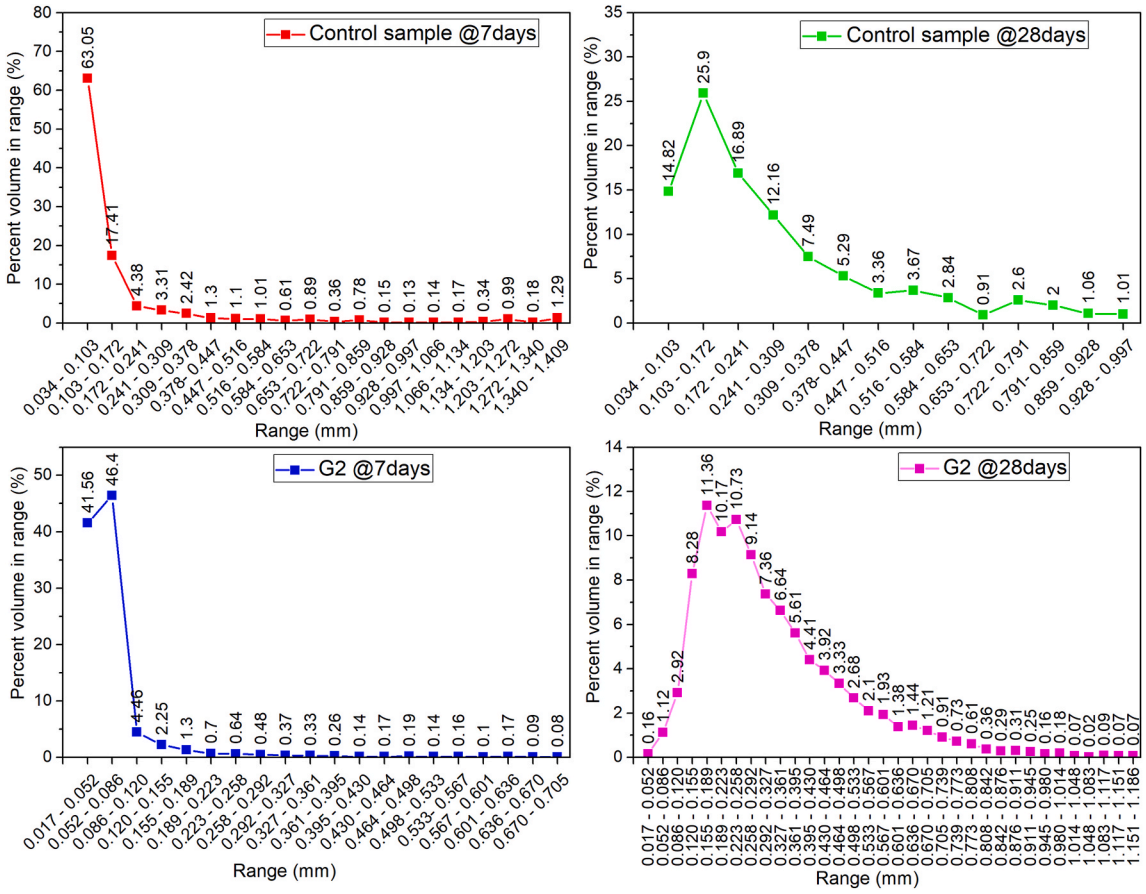

Fig. 8. Pore size distribution by μ-CT of the control sample and G2 sample at 7 and 28 days.

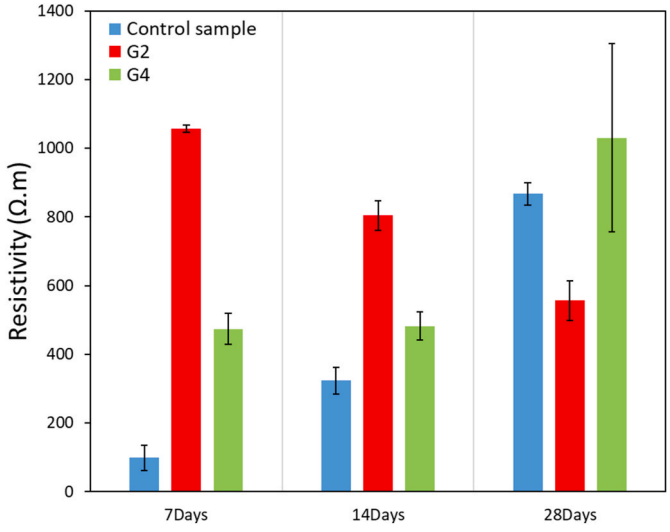

Fig. 9. Electrical resistivity of GNP-modified mortars hardened at 7, 14, and 28 days.

$$Z_{CPE} = \frac{1}{Q(j\omega)^n} \quad (3)$$

where:

j = $\sqrt{-1}$, Q is the pseudo-capacitive coefficient, ω is the angular frequency, and n can adopt values between 0 and 1 (i.e. n = 0 represents the pure resistor and n = 1 represents the perfect capacitor) [53].

Referring to Fig. 10, *Rs* represents the resistance to the ionic current through the pore solution acting as an electrolyte (*pore solution* resistance). It is accepted that *Rs* in CBMs is inversely proportional to the porosity and the pore solution concentration [54].

Based on the adopted two-point electrode method, *R1* and *Q1* represent, respectively, the *charge transfer resistance* and the *double-layer capacitance* between the mortar and the electrodes.

The cement matrix has limited conductivity and it acts as a dielectric if placed in contact with metal electrodes and if an AC signal is applied.

To evaluate the effect of the high conductivity nanofiller on the electrical properties of the investigated nanocomposites, a further conductive path needs to be considered.

Because of *charge transfer resistance* (*R2*) and *double layer capacitance (Q2)* at the interphase between the GNPs and the cement matrix, a second RC circuit should be included in the equivalent circuit [54–56].

For all the samples, progressive cement hydration clearly led to increased *pore solution resistance* (*Rs*) due to the decreased amount of the evaporable free water, accompanied by reduced interconnectivity of the capillary pore network [29,57] (Table 4). Thus, in the case of the neat mortar, the hydration process led to the previously observed trend of electrical resistivity (Fig. 9).

Interestingly, the GNP-modified mortars hardened for 7 days showed higher *Rs* values with respect to those obtained for the neat sample (1395 Ω, 1408 Ω, and 1643 Ω for the control sample, G2 and G4, respectively). The effect, remarkable only in the case of samples loaded with the higher aspect ratio *G4Nan*, has to be associated with an accelerated hydration process promoted by the heterogeneous nucleation of C–S–H onto the surface of the wide and wrinkled GNPs (Figs. 2

Table 4
Fitting parameters of the equivalent circuit simulation for hardened GNP-modified mortars and control sample (CS) at 7, 14, and 28 days.

Sample	Rs (Ω)	R1 (Ω)	Q1 ($s^{n2}\Omega^{-1}$)	N1 (−)	R2 (Ω)	Q2 ($s^{n2}\Omega^{-1}$)	N2 (−)	Chi-Sq	Sum-Sq
CS-7d	1395	9809	1.953E-4	0.54084	–	–	–	0.0061659	0.60426
CS-14d	2080	36173	3.018E-5	0.74776	–	–	–	0.013782	1.6814
CS-28d	4562	90 462	1.5825E-5	0.77532	–	–	–	0.0011783	0.084837
G2-7d	1408	363	1.8388E-6	0.68223	112 350	1.4158E-5	0.81357	0.0030487	0.36889
G2-14d	1528	1834	4.7726E-6	0.59263	83 540	1.5061E-5	0.78162	0.00097104	0.1175
G2-28d	1589	2456	9.9347E-6	0.53865	54 188	3.0168E-5	0.76687	0.00057684	0.069798
G4-7d	1643	23 958	3.3771E-5	0.79663	35 622	1.0216E-4	0.75125	0.00050585	0.047044
G4-14d	2069	23 839	3.5829E-5	0.8361	29 540	1.237E-4	0.77833	0.00010042	0.0069293
G4-28d	2610	111 440	1.0575E-5	0.81534	26 199	3.1928E-4	0.93945	0.00073611	0.04375

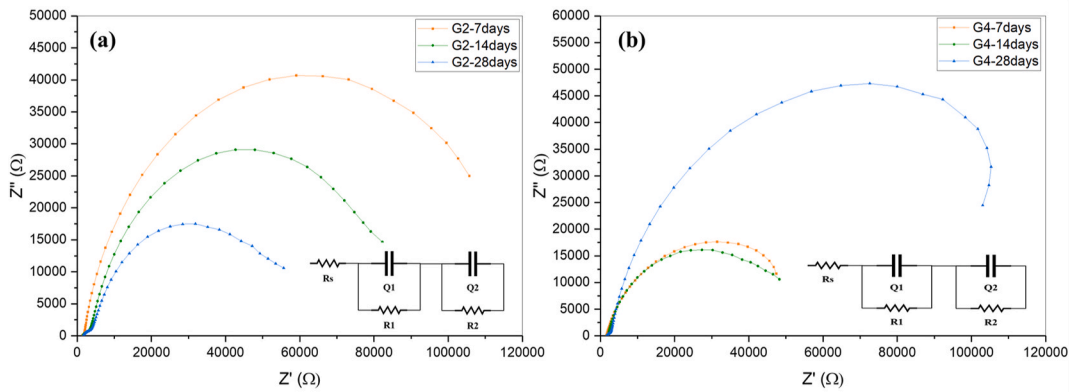

Fig. 10. *Rs*: resistance of pore solution; *R1*: charge transfer resistance between mortar and electrodes; *R2*: charge transfer resistance between GNPs and mortar; *Q1*: double-layer capacitance between the mortar and electrodes; *Q2* double-layer capacitance between GNPs and mortar (a) *G2Nan*-modified mortar and (b) *G4Nan*-modified mortar.

and 6). An opposite trend was observed in the case of samples cured for 14 and 28 days, the *Rs* values being, respectively, 2080 Ω and 4562 Ω, 1528 Ω and 1589 Ω, 2069 Ω and 2610 Ω for the control sample, G2, and G4 (Table 4). This result suggests that the GNP-modified mortars maintained during the hydration time a higher degree of pore interconnectivity with respect to the neat sample, with *G2Nan* being more efficient than *G4Nan* [57,58].

Regarding *R1*, a progressive and expected increasing trend with the hydration time was obtained for both the neat mortar and G2, whereas G4 showed a distinctly different behavior (Table 4).

However, the *R1* values of *G2Nan*-modified mortar at 7, 14, and 28 days are much lower compared to those of the respective control samples. This result clearly indicates a remarkable enhancement of charge transport properties promoted by the nanofiller and associated with the increase of the double-layer capacitance (*Q1*).

In the case of G4, both *R1* and *Q1* values are almost the same at 7 and 14 days. At 28 days, *R1* sharply increases and *Q1* diminishes, showing a decrease of charge transport properties. It is reasonable to associate such behavior with the presence of microstructural inhomogeneities, which is also suggested from the high standard deviation of resistivity value of G4 at 28 days reported in Fig. 9.

Regarding *R2*, a progressively decreasing trend with the aging time was obtained for the two GNP-modified mortars (Table 4), which is associated with the ongoing hydration of cement and the resulting development of the interfacial bonding between filler and cement hydration products that promotes charge transfer.

Moreover, since the *R2* values of G4 are much lower compared to G2, the conclusion can be drawn that the charge transfer between nanoplatelets and the cementitious matrix was greatly advantaged by the presence of the higher aspect ratio nanofiller (Table 1).

Finally, the *double-layer capacitance* (*Q2*) improved with hydration time for both GNP-modified mortars, and the *Q2* values of *G4Nan*-modified mortars were ten times higher compared to the *G2Nan*-modified ones. Such an occurrence might be explained by considering an improved interfacial adhesion strength and/or a larger filler/matrix interface. Moreover, as reported in the literature, GNPs – owing to their bidimensional shape – are more effective than other carbon-based nanofillers in the enhancement of interface conduction and capacitance in cementitious nanocomposites, so the better electrical properties at the interface of G4 have to be associated with the higher aspect ratio of the *G4Nan* filler [49]. However, such a contribution to the overall electrical conductivity of the composites is negligible with respect to ionic, tunneling, and contacting conduction, since the conductivity of the cementitious matrix is several orders lower than that of the pore solution [59,60].

3.6. GNP-modified nanocomposites: thermal conductivity

It is well known that the durability of CBMs is deeply affected by early-age cracking. Many studies focused on different strategies to improve the thermal conductivity of the cementitious products aimed to dissipate the heat arising from the hydration process, leading to reduced temperature gradients and, consequently, lower thermal stresses that are mainly responsible for the early-age cracking [15,61].

GNPs have excellent in-plane thermal conductivity ranging between 3080 and 5300 W/m·K, depending on: *(i)* structural defects, either at the surface or at the boundaries; and *(ii)* the number of layers, acting as channels for the phonon scattering [62–64].

The results of thermal conductivity measurements performed on the investigated GNP-modified mortars are reported in Fig. 11.

Premixed mortars, reinforced with 0.01% (by weight of cement) of *G2Nan* and *G4Nan*, showed improved thermal conductivity compared to the control sample, by 60% and 32%, respectively. The highest thermal conductivity (1.37 W/m·K) was recorded for *G2Nan*-modified mortar; a comparable value (1.33 W/m K) has been previously reported for the same mortar modified with 0.01% of nG [28].

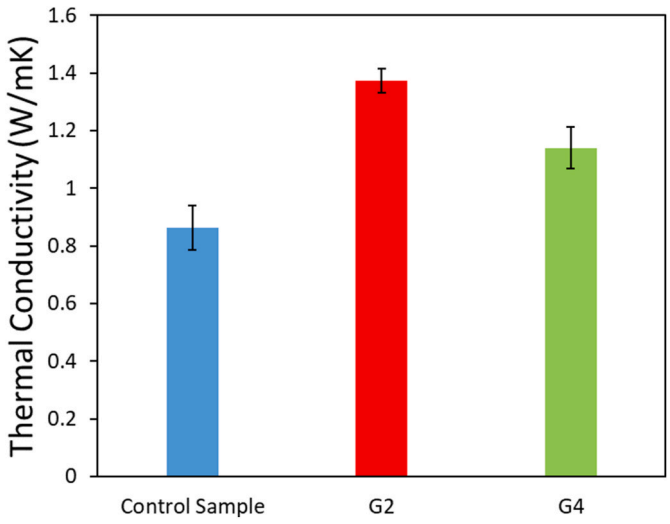

Fig. 11. Thermal conductivity of GNP-modified mortars at 28 days.

Several studies demonstrated that the incorporation of GNPs enhances the thermal conductivity of the resulting cement-based nanocomposites, with the amount of required nanofiller usually varying between 1 and 5% [15,49,65]. For example, cementitious nanocomposites loaded with 2% GNPs (by weight of cement) led to materials characterized by thermal conductivity of 1.14 W/m·K, corresponding to +46% with respect to the neat material [49]. Furthermore, 1.22 W/m·K thermal conductivity was reached by loading cementitious materials with 1% volume GNPs [66].

GNP-modified nanocomposites are phonon-based heat conductors. Their thermal conductivity depends on distinct issues, mainly: *(i)* the intrinsic thermal conductivity of both the nanofiller and the cementitious matrix (including the contribution of the pore refinement effect promoted by the nanofiller that positively affects the thermal conductivity); *(ii)* the amount, morphology, texture, thickness and aspect ratio of the nanoplatelets; and (*iii*) the dispersion degree of the conductive filler [66].

The dispersion degree of the GNPs plays a pivotal role in the enhancement of the thermal conduction: only a uniform filler dispersion allows the development of effective thermally conductive pathways. Moreover, fillers with a higher aspect ratio can form more continuous thermally conductive pathways in the matrix and, thus, are more effective in enhancing the thermal transfer [67].

In fact, since the phonon scattering occurs at the interface between the matrix and the nanofiller, a high thermal resistance at such a microscopic scale becomes a serious issue, hindering the improvement to the thermal conductivity of the nanocomposite [68]. In this respect, it has been demonstrated that GNP-modified polymeric composites show higher improvement in thermal conductivity and heat dissipation ability for GNPs of larger lateral size and greater thickness, associated with the minimized matrix/nanofiller interface [69].

On such a basis, it can be concluded that the high thermal conductivity of the investigated GNP-modified mortar samples has to be mainly attributed to the achievement of an adequate dispersion degree, and a favorable orientation of nanofiller in the cementitious matrix. The effect is optimized by the incorporation of low aspect ratio GNPs (*G2Nan*) that minimize the thermal interfacial resistance.

4. Conclusions

The study aimed to investigate the overall impact of high aspect ratio (*G4Nan*) and low aspect ratio (*G2Nan*) GNPs on the properties of the resulting cement-based nanocomposites hardened for 7, 14, and 28 days. Based on a previous study, only a minimum dosage of nanofiller was considered (*i.e.* 0.01% by weight of cement).

The following conclusive statements were gathered:

- The rheological behavior of the fresh GNP-modified admixtures was slightly affected by the incorporation of nanofiller, where *G4Nan* induced a smooth self-lubrication effect.
- Density enhancement was observed for all GNP-modified mortars – it reached about 12% (at 28 days) – and a negligible difference was observed for nanocomposites reinforced with *G4Nan* or *G2Nan*.
- G2 and G4 samples showed a moderate compressive strength enhancement (6% and 14%, respectively) compared to the control sample, while the impact on flexural strengthening was even milder (2% and 4%, respectively) (at 28 days). The higher effectiveness of *G4Nan* platelets was attributed to the higher aspect ratio that is responsible for several positive effects at the microscopic scale including mechanical interlocking, bridging effect, and pore refining.
- According to the SEM investigation, the overall microstructure of the GNP-modified mortars was nearly unaffected by the incorporation of the nanoplatelets (at 28 days). However, the μ-CT technique clearly pointed out the distinctively different impact of GNPs on the evolution of the pore network over hardening time.
- Thermal conductivity of the cementitious nanocomposites was remarkably promoted by *G2Nan* and *G4Nan,* increasing by 60% and 32%, respectively (at 28 days) compared to control sample. The lower aspect ratio *G2Nan* led to a reduction of the interfacial area between the matrix and the nanofiller and, consequently, minimized the thermal interfacial resistance.
- The impact of *G2Nan* and *G4Nan* on electrical resistivity was undoubtedly different. *G2Nan*-modified mortars showed a progressive decreasing trend with the hydration time and reached a reduction of 36% at 28 days compared to the control sample. *G4Nan*-modified mortars showed the opposite trend; the electrical resistivity at 28 days was comparable to that of the control sample.

Such results are associated to a more homogeneous dispersion of the lower aspect ratio *G2Nan*, leading to a favorable distribution and/or orientation of the conductive nanofiller in the cementitious matrix, and a higher degree of pore connectivity promoting ionic conduction.

In light of the above points, it can be concluded that: *(i) G2Nan* platelets (aspect ratio $1.786 \cdot 10^3$) achieved adequate dispersion and favorable orientation within the cementitious matrix resulting in fresh admixtures of nearly preserved workability and hardened cementitious nanocomposites characterized by improved density (12%), slight strengthening (R_c 6% and R_b 2%), remarkably enhanced thermal conductivity (60%), and reduced electrical resistivity (36%). The addition of the higher aspect ratio GNPs (*G4Nan*, aspect ratio $5.250 \cdot 10^3$)- despite resulting in slight advantageous in terms of workability, strength, and thermal conductivity-did not significantly affect the electrical resistivity of the resulting cementitious nanocomposites.

Funding

This research did not receive any specific grant from funding agencies in the public, commercial, or not-for-profit sectors.

Declaration of competing interest

The authors declare that they have no known competing financial interests or personal relationships that could have appeared to influence the work reported in this paper.

Acknowledgments

The authors wish to thank prof. Alessandra D'Epifanio of the Department of Chemical Science and Technologies - University of Rome

Tor Vergata for the availability of EIS measurement apparatus.

References

[1] Cement market size, share, and trends analysis report by product (Portland, others), by application (residential, non-residential/infrastructure), by region, vendor landscape, and segment forecasts, 2018 – 2025. https://www.researchandmarkets.com/research/qld898/2018_cement?w=5.

[2] S. Ghourchian, M. Wyrzykowski, P. Lura, A practical approach for reducing the risk of plastic shrinkage cracking of concrete, RILEM Tech. Lett. 2 (2017) 40–44, https://doi.org/10.21809/rilemtechlett.2017.45.

[3] Md Safiuddin, A.B.M. Amrul Kaish, C.-O. Woon, S.N. Raman, Early-age cracking in concrete: causes, consequences, remedial measures, and recommendations, Appl. Sci. 8 (2018) 1730. http://doi:10.3390/app8101730.

[4] B. Li, J. Mao, T. Nawa, T. Han, Mesoscopic damage model of concrete subjected to freeze-thaw cycles using mercury intrusion porosimetry and differential scanning calorimetry (MIP-DSC), Construct. Build. Mater. 147 (2017) 79–90, https://doi.org/10.1016/j.conbuildmat.2017.04.136.

[5] M.J. Al-Kheetan, M. Al-Tarawneh, S.H. Ghaffar, M. Chougan, Y.S. Jweihan, M. M. Rahman, Resistance of Hydrophobic Concrete with Different Moisture Contents to Advanced Freeze–Thaw Cycles Structural Concrete, 2020, https://doi.org/10.1002/suco.202000214.

[6] B. Wang, R. Jiang, Z. Wu, Investigation of the mechanical properties and microstructure of graphene nanoplatelet-cement composite, Nanomaterials 6 (2016) 200, https://doi.org/10.3390/nano6110200.

[7] H. Yang, H. Cui, W. Tang, Z. Li, N. Han, F. Xing, A critical review on research progress of graphene/cement based composites, Compos. Part A 102 (2017) 273–296, https://doi.org/10.1016/j.compositesa.2017.07.019.

[8] S. Lv, Y. Ma, C. Qiu, T. Sun, J. Liu, Q. Zhou, Effect of graphene oxide nanosheets of microstructure and mechanical properties of cement composites, Construct. Build. Mater. 49 (2013) 121–127, https://doi.org/10.1016/j.conbuildmat.2013.08.022.

[9] H. Du, S.D. Pang, Enhancement of barrier properties of cement mortar with graphene nanoplatelet, Cement Concr. Res. 76 (2015) 10–19, https://doi.org/10.1016/j.cemconres.2015.05.007.

[10] M. Chougan, S.H. Ghaffar, M. Jahanzat, A. Albar, N. Mujaddedi, R. Swash, The influence of nano-additives in strengthening mechanical performance of 3D printed multi-binder geopolymer composites, Construct. Build. Mater. 250 (2020) 118928, https://doi.org/10.1016/j.conbuildmat.2020.118928.

[11] A. Mohammed, J.G. Sanjayan, W.H. Duan, A. Nazari, Graphene oxide impact on hardened cement expressed in enhanced freeze–thaw resistance, J. Mater. Civ. Eng. 28 (2016), 04016072, https://doi.org/10.1061/(ASCE)MT.1943-5533.0001586.

[12] S. Du, J. Wu, O. AlShareedah, X. Shi, Nanotechnology in cement-based materials: a review of durability, modeling, and advanced characterization, Nanomaterials 9 (2019) 1213, https://doi.org/10.3390/nano9091213.

[13] G. Chen, M. Yang, L. Xu, Y. Zhang, Y. Wang, Graphene nanoplatelets impact on concrete in improving freeze-thaw resistance, Appl. Sci. 9 (2019) 3582, https://doi.org/10.3390/app9173582.

[14] J. Wang, Y. Xu, X. Wu, P. Zhang, S. Hu, Advances of graphene- and graphene oxide modified cementitious materials, Nanotechnol. Rev. 9 (2020) 465–477, https://doi.org/10.1515/ntrev-2020-0041.

[15] Q. Zheng, B. Han, X. Cui, X. Yu, J. Ou, Graphene-engineered cementitious composites: small makes a big impact, Nanomater. Nanotechnol. 7 (2017) 1–18, https://doi.org/10.1177/1847980417742304.

[16] N. Jaitanong, S. Narksitipan, A. Ngamjarurojana, A. Chaipanich, Influence of graphene nanoplatelets on morphological and electrical properties of silica fume blended cement – piezoelectric ceramic composite, Ceram. Int. 44 (2018) S137–S140, https://doi.org/10.1016/j.ceramint.2018.08.131.

[17] R. Bogue, Smart materials: a review of recent developments, Assemb. Autom. 32 (2012) 3–7, https://doi.org/10.1108/01445151211198674.

[18] D.D.L. Chung, Piezoresistive cement-based materials for strain sensing, J. Intell. Mater. Syst. Struct. 13 (2002) 599–609, https://doi.org/10.1106/104538902031861.

[19] F. Inam, B.R. Bhat, T. Vo, W.M. Daoush, Structural health monitoring capabilities in ceramic–carbon nanocomposites, Ceram. Int. 40 (2014) 3793–3798, https://doi.org/10.1016/j.ceramint.2013.09.039.

[20] J. Tao, J. Wang, Q. Zeng, A comparative study on the influences of CNT and GNP on the piezoresistivity of cement composites, Mater. Lett. 259 (2020) 126858, https://doi.org/10.1016/j.matlet.2019.126858.

[21] M.S. Konsta-Gdoutos, C.A. Aza, Self sensing carbon nanotube (CNT) and nanofiber (CNF) cementitious composites for real time damage assessment in smart structures, Cement Concr. Compos. 53 (2014) 162–169, https://doi.org/10.1016/j.cemconcomp.2014.07.003.

[22] D.-Y. Yoo, I. You, S.-J. Lee, Electrical properties of cement-based composites with carbon nanotubes, graphene, and graphite nanofibers, Sensors 17 (2017) 1064, https://doi.org/10.3390/s17051064.

[23] T. Evgin, A. Turgut, G. Hamaoui, Z. Spitalsky, N. Horny, M. Micusik, M. Chirtoc, M. Sarikanat, M. Omastova, Size effects of graphene nanoplatelets on the properties of high-density polyethylene nanocomposites: morphological, thermal, electrical, and mechanical characterization, Beilstein J. Nanotechnol. 11 (2020) 167–179, https://doi.org/10.3762/bjnano.11.14.

[24] R. Sengupta, M. Bhattacharya, S. Bandyopadhyay, et al., A review on the mechanical and electrical properties of graphite and modified graphite reinforced polymer composites, Prog. Polym. Sci. 36 (2011) 638–670.

[25] Klaus D. Sattler CRC Press, 6 apr 2016 - 735 pagine, Carbon Nanomaterials Sourcebook: Nanoparticles, Nanocapsules, Nanofibers, Nanoporous Structures, and Nanocomposites, Volume II, Volume 2. p. 678.

[26] M. Chougan, E. Marotta, F.R. Lamastra, F. Vivio, G. Montesperelli, U. Ianniruberto, A. Bianco, A systematic study on EN-998-2 premixed mortars modified with graphene-based materials, Construct. Build. Mater. 227 (2019) 116701, https://doi.org/10.1016/j.conbuildmat.2019.116701.

[27] P. Cataldi, A. Athanassiou, I.S. Bayer, Graphene nanoplatelets-based advanced materials and recent progress in sustainable applications, Appl. Sci. 8 (2018) 1438. https://doi:10.3390/app8091438.

[28] M. Chougan, E. Marotta, F.R. Lamastra, F. Vivio, G. Montesperelli, U. Ianniruberto, S.H. Ghaffar, M.J. Al-kheetan, A. Bianco, High performance cementitious nanocomposites: the effectiveness of nano-Graphite (nG), Construct. Build. Mater. 259 (2020) 119687, https://doi.org/10.1016/j.conbuildmat.2020.119687.

[29] T. Ch Madhavi, S. Annamalai, Electrical conductivity of concrete, ARPN J. Eng. Appl. Sci. 11 (2016) 5979–5982.

[30] X. Li, L. Wang, Y. Liu, W. Li, B. Dong, W.H. Duan, Dispersion of graphene oxide agglomerates in cement paste and its effects on electrical resistivity and flexural strength, Cement Concr. Compos. 92 (2018) 145–154, https://doi.org/10.1016/j.cemconcomp.2018.06.008.

[31] Z. Baig, O. Mamat, M. Mustapha, A. Mumtaz, K.S. Munir, M. Sarfraz, Investigation of tip sonication effects on structural quality of graphene nanoplatelets (GNPs) for superior solvent dispersion, Ultrason. Sonochem. 45 (2018) 133–149, https://doi.org/10.1016/j.ultsonch.2018.03.007.

[32] A. Alatawna, M. Birenboim, R. Nadiv, M. Buzaglo, S. Peretz-Damari, A. Peled, O. Regev, R. Sripada, The effect of compatibility and dimensionality of carbon nanofillers on cement composites, Construct. Build. Mater. 232 (2020) 117141, https://doi.org/10.1016/j.conbuildmat.2019.117141.

[33] E.C. Bingham, Fluidity and Plasticity, McGraw-Hill Book Co. Inc., New York, NY, USA, 1922, p. 440.

[34] F.-J.R. Hernández, Rheological behavior of fresh cement pastes, Fluids 3 (2018) 106. https://doi:10.3390/fluids3040106.

[35] S.K.U. Rehman, S. Kumarova, S.A. Memon, M.F. Javed, M. Jameel, A review of microscale, rheological, mechanical, thermoelectrical and piezoresistive properties of graphene based cement composite, Nanomaterials 10 (2020) 2076. https://doi:10.3390/nano10102076.

[36] C.M. Pederneiras, R. Veiga, J. de Brito, Rendering mortars reinforced with natural sheep's wool fibers, Materials 12 (2019) 3648. https://doi:10.3390/ma12223648.

[37] J. Tao, X. Wang, Z. Wang, Q. Zeng, Graphene nanoplatelets as an effective additive to tune the microstructures and piezoresistive properties of cement-based composites, Construct. Build. Mater. (2019) 665–678, https://doi.org/10.1016/j.conbuildmat.2019.03.173.

[38] M. Yang, G. Chen, N. Cao, Y. Zhang, Y. Wang, Effect of graphenene nanoplatelets on microstructure and properties of cement mortar under simulated acid rain, IOP Conf. Ser. Mater. Sci. Eng. 631 (2019), 022036. https://doi:10.1088/1757899X/631/2/022036.

[39] W. Meng, K.H. Khayat, Effect of graphite nanoplatelets and carbon nanofibers on rheology, hydration, shrinkage, mechanical properties, and microstructure of UHPC, Cement Concr. Res. 105 (2018) 64–71, https://doi.org/10.1016/j.cemconres.2018.01.001.

[40] H. Peng, Y. Ge, C.S. Cai, Y. Zhang, Z. Liu, Mechanical properties and microstructure of graphene oxide cement-based composites, Construct. Build. Mater. 194 (2019) 102–109, https://doi.org/10.1016/j.conbuildmat.2018.10.234.

[41] M.T. Müller, K. Hilarius, M. Liebscher, D. Lellinger, I. Alig, Petra pötschke, effect of graphite nanoplate morphology on the dispersion and physical properties of polycarbonate based composites, Materials 10 (2017) 545. https://doi:10.3390/ma10050545.

[42] S. Bai, L. Jiang, N. Xu, M. Jin, S. Jiang, Enhancement of mechanical and electrical properties of graphene/cement composite due to improved dispersion of graphene by addition of silica fume, Construct. Build. Mater. 164 (2018) 433–441, https://doi.org/10.1016/j.conbuildmat.2017.12.176.

[43] A. du Plessi, B.J. Olawuyi, W.P. Boshoff, S.G. le Roux, Simple and fast porosity analysis of concrete using X-ray computed tomography, Mater. Struct. 49 (2016) 553–562. https://doi:10.1617/s11527-014-0519-9.

[44] N. Bossa, P. Chaurand, J. Vicente, D. Borschneck, C. Levard, O. Aguerre-Chariol, J. Rose, Micro- and nano-X-ray computed-tomography: a step forward in the characterization of the pore network of a leached cement paste, Cement Concr. Res. 67 (2015) 138–147, https://doi.org/10.1016/j.cemconres.2014.08.007.

[45] E. Gallucci, K. Scrivener, A. Groso, M. Stampanoni, G. Margaritondo, 3D experimental investigation of the microstructure of cement pastes using synchrotron X-ray microtomography (μCT), Cement Concr. Res. 37 (2007) 360–368, https://doi.org/10.1016/j.cemconres.2006.10.012.

[46] Y. Song, J-w Zhou, Z-n Bian, G-z Dai, Pore structure characterization of hardened cement paste by multiple methods, Ann. Mater. Sci. Eng. (2019), 3726953, https://doi.org/10.1155/2019/3726953.

[47] M.H.N. Yio, H.S. Wong, N.R. Buenfeld, 3D pore structure and mass transport properties of blended cementitious materials, Cement Concr. Res. 117 (2019) 23–37, https://doi.org/10.1016/j.cemconres.2018.12.007.

[48] A. D'Alessandro, A.L. Materazzi, F. Ubertini, Nanotechnology in Cement-Based Construction, CRC Press, Jenny Standford Publishing Pte. Ltd., Singapore, 2020.

[49] A.L. Pisello, A. D'Alessandro, S. Sambuco, M. Rallini, F. Ubertini, F. Asdrubali, A. L. Materazzi, F. Cotana, Multipurpose experimental characterization of smart nanocomposite cement-based materials for thermal-energy efficiency and strain-sensing capability, Sol. Energ. Mat. Sol. C. 161 (2017) 77–88, https://doi.org/10.1016/j.solmat.2016.11.030.

[50] S. Bai, L. Jiang, Y. Jiang, M.J. Shaobo, J.D. Tao, Research on electrical conductivity of graphene/cement composites, Adv. Cement Res. 32 (2020) 45–52, https://doi.org/10.1680/jadcr.16.00170.
[51] B. Dong, Q. Qiu, J. Xiang, C. Huang, F. Xing, N. Ha, Study on the carbonation behavior of cement mortar by electrochemical impedance spectroscopy, Materials 7 (2014) 218–231. https://doi:10.3390/ma7010218.
[52] X. Hu, C. Shi, X. Liu, J. Zhang, G. de Schutter, A review on microstructural characterization of cement-based materials by AC impedance spectroscopy, Cement Concr. Compos. 100 (2019) 1–14, https://doi.org/10.1016/j.cemconcomp.2019.03.018.
[53] C.G. Berrocal, K. Hornbostel, M.R. Geiker, I. Lofgren, K. Lundgren, D.G. Bekas, Electrical resistivity measurements in steel fibre reinforced cementitious materials, Cement Concr. Compos. 89 (2018) 216–229, https://doi.org/10.1016/j.cemconcomp.2018.03.015.
[54] S. Sun, S. Ding, B. Han, S. Dong, X. Yu, D. Zhou, J. Ou, Multi-layer graphene-engineered cementitious composites with multifunctionality/intelligence, Compos. Part B 129 (2017) 221–232, https://doi.org/10.1016/j.compositesb.2017.07.063.
[55] W-w Li, W-m Ji, G.- h Fang, Y-q Liu, F. Xing, Y-k Liu, B-q Dong, Electrochemical impedance interpretation for the fracture toughness of carbon nanotube/cement composites, Construct. Build. Mater. 114 (2016) 499–505, https://doi.org/10.1016/j.conbuildmat.2016.03.215.
[56] P. Payakaniti, S. Pinitsoontorn, P. Thongbai, V. Amornkitbamrung, P. Chindaprasirt, Electrical conductivity and compressive strength of carbon fiber reinforced fly ash geopolymeric composites, Construct. Build. Mater. 135 (2017) 164–176, https://doi.org/10.1016/j.conbuildmat.2016.12.198.
[57] A. Xu, Y. Weng, R. Zhao, Permeability and equivalent circuit model of ionically conductive mortar using electrochemical workstation, Materials 13 (2020) 1179, https://doi.org/10.3390/ma13051179.
[58] H.W. Reinhardt, C.U. Grosse, Report 31: Advanced Testing of Cement-Based Materials during Setting and Hardening - Report of RILEM Technical Committee 185-ATC, RILEM Publications, 2005.
[59] K. Liang, X. Zeng, X. Zhou, F. Qu, P. Wang, A New Model for the Electrical Conductivity of Cement-Based Material by Considering Pore Size Distribution, Magazine of Concrete Research, 2017, https://doi.org/10.1680/jmacr.16.00535. Paper 1600535.
[60] R.T. Coverdale, B.J. Christensen, H.M. Jennings, T.O. Mason, D.P. Bentz, E. J. Garboczi, Interpretation of impedance spectroscopy of cement paste via computer modelling, J. Mater. Sci. 30 (1995) 712–719, https://doi.org/10.1007/BF00356331.
[61] B. Klemczak, A. Jędrzejewska, Early age thermal and shrinkage cracks in concrete structures - description of the problem, Architect. Civ. Environ. Eng. 3 (2011) 55–70.
[62] K. Chu, C.- c Jia, W-s Li, Effective thermal conductivity of graphene-based composites, Appl. Phys. Lett. 101 (2012) 121916, https://doi.org/10.1063/1.4754120.
[63] A.A. Balandin, S. Ghosh, W. Bao, I. Calizo, D. Teweldebrhan, F. Miao, C.N. Lau, Superior thermal conductivity of single-layer graphene, Nano Lett. 8 (2008) 902–907, https://doi.org/10.1021/nl0731872.
[64] S.K. Jaćimovski, M. Bukurov, J.P. Šetrajčić, D.I. Raković, Phonon thermal conductivity of graphene, Superlattice, Microst 88 (2015) 330–337, https://doi.org/10.1016/j.spmi.2015.09.027.
[65] M. Du, H. Jing, Y. Gao, H. Su, H. Fang, Carbon nanomaterials enhanced cement-based composites: advances and challenges, Nanotechnol. Rev. 9 (2020) 115–135, https://doi.org/10.1515/ntrev-2020-0011.
[66] X. Cui, S. Sun, B. Han, X. Yu, J. Ouyang, S. Zeng, J. Ou, Mechanical, thermal and electromagnetic properties of nanographite platelets modified cementitious composites, Compos. Part A 93 (2017) 49–58, https://doi.org/10.1016/j.compositesa.2016.11.017.
[67] C. Min, D. Yu, J. Cao, G. Wang, L. Feng, A graphite nanoplatelet/epoxy composite with high dielectric constant and high thermal conductivity, Carbon 55 (2013) 116–125, https://doi.org/10.1016/j.carbon.2012.12.017.
[68] A. Caradonna, C. Badini, E. Padovano, M. Pietroluongo, Electrical and thermal conductivity of epoxy-carbon filler composites processed by calendaring, Materials 12 (2019) 1522, https://doi.org/10.3390/ma12091522.
[69] H.S. Kim, H.S. Bae, J. Yu, S.Y. Kim, Thermal conductivity of polymer composites with the geometrical characteristics of graphene nanoplatelets, Sci. Rep. 6 (2016) 26825, https://doi.org/10.1038/srep26825.